[4] Kacprzynski, J. J., Ohman, L. H., Garabedian, P. R., and Korn, D. G., "Analysis of the Flow Past the Shockless Lifting Airfoil in Design and Off-Design Conditions," AIAA Paper 71-567, Palo Alto, Calif., 1971.

[5] Murman, E. M. and Cole, J. D., "Calculation of Plane Steady Transonic Flows," *AIAA Journal*, Vol. 9, No. 1, Jan. 1971, pp. 114–121.

[6] Krupp, J. A. and Murman, E. M., "The Numerical Calculation of Steady Transonic Flows Past Thin Lifting Airfoils and Slender Bodies," AIAA Paper 71-566, Palo Alto, Calif., 1971.

[7] Murman, E. M. and Krupp, J. A., "Solution of the Transonic Potential Equation Using a Mixed Finite Difference System," *Lecture Notes in Physics*, Vol. 8, Springer-Verlag, Berlin, 1971.

[8] Bailey, F. R. and Steger, J. L., "Relaxation Techniques for Three-Dimensional Transonic Flow About Wings," AIAA Paper 72-189, San Diego, Calif., 1972.

[9] Steger, J. L. and Lomax, H., "Generalized Relaxation Methods Applied to Problems in Transonic Flow," *Lecture Notes in Physics*, Vol. 8, Springer-Verlag, Berlin, 1971.

Experimental Determination of the Aeroacoustic Environment about a Slender Cone

A. MARTELLUCCI,* L. CHAUMP,† AND D. ROGERS‡
General Electric Company, Philadelphia, Pa.

AND

D. SMITH§
Wright-Patterson Air Force Base, Ohio

Acoustic pressure fluctuation and heat-transfer data have been obtained on a 7.2° half-angle cone. Measurements were obtained at Mach 4, 8, and 10 for several values of the freestream Reynolds number and cone angle of attack, and three bluntness ratios. Natural transition was achieved in all cases. Methods of data acquisition and analysis are discussed. Selected boundary-layer root-mean-square (rms) pressure fluctuation data and transition front shape, deduced from the heat-transfer data, are presented. Heat transfer, rms pressure, and turbulent velocity profile exponent data are all shown to peak near the end of transition.

Nomenclature

C_f = skin-friction coefficient
db = decibel (reference pressure 0.0002 μbars)
E = end of transition (peak $\dot{q}$)
H_0, h_w = stagnation and wall enthalpy, respectively
L = model length
M = Mach number
n = velocity profile exponent
0 = onset of transition (minimum $\dot{q}$)
$\tilde{P}$ = rms fluctuating pressure
q = dynamic pressure
$\dot{q}$ = heat-transfer rate
R = radius
Re/ft = unit Reynolds number per foot
Re_s = local wetted length Reynolds number
S = wetted length along cone
S_T = Stanton number
T = temperature
u = axial velocity
x = axial coordinate
y = coordinate normal to surface
α = angle of attack
δ = boundary-layer thickness
γ = ratio of specific heats
θ_c = cone half angle
μ = molecular viscosity
ρ = density

Subscripts

aw = adiabatic wall
B = model base
e = edge of boundary layer
L = edge of laminar sublayer
N = nose
T = transition onset
w = conditions at wall
∞ = freestream conditions

Presented as Paper 72-706 at the AIAA 5th Fluid and Plasma Dynamics Conference, Boston, Mass., June 26–28, 1972; received August 7, 1972; revision received November 27, 1972. This research was sponsored by the Air Force Flight Dynamics Laboratory (AFFDL), Wright-Patterson Air Force Base, Ohio under contract F33615-71-C-1245. The authors wish to acknowledge the efforts of F. George and C. Davies for their assistance in fabrication and assembly of the model, and to A. Monfort for his contribution in the data analysis and evaluation.

Index categories: Supersonic and Hypersonic Flow; Boundary-Layer Stability and Transition.

* Consultant, Aerothermodynamics Laboratory. Associate Fellow AIAA.

† Manager, Structural Mechanics Laboratory. Member AIAA.

‡ Supervising Engineer—Instrumentation. Member AIAA.

§ Project Engineer, Air Force Flight Dynamics Laboratory.

I. Introduction

DURING re-entry into the Earth's atmosphere, vehicles are subjected to intense fluctuating aerodynamic pressures. As a result, significant vibration response can occur affecting the performance of components within the vehicle. In order to accurately assess this problem, it is necessary to define the nature of the acoustic environment associated with turbulent flow over the re-entry vehicle. This has become more important as mission requirements have resulted in higher velocities at relatively lower altitudes. Predictions based on available low Mach number data indicate that sound pressure levels on the order of 190 db may be encountered.

The purpose of the program undertaken in the present study was to measure the aeroacoustic environment on the surface

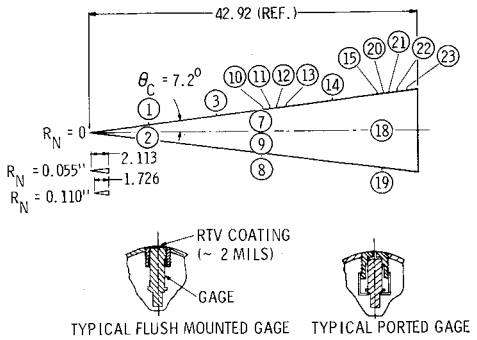

Fig. 1 Model schematic.

of a smooth, conical body and use the results to upgrade current analytic formulations for the prediction of the sound pressure levels. In addition to measuring the noise levels, it was also desirable to obtain spatial information which would permit the determination of correlation functions, a significant factor in computing structural response. Yet another item of concern was the acoustic environment during transitional as well as fully developed turbulent flow.

The test program briefly discussed in this paper summarizes a portion of the results, outlining the considerations made in test model and instrumentation selection, exploratory testing for transition, data acquisition, evaluation, and correlation. Finally, a comparison of data with current theory is made, and possible refinements are discussed. One important finding was the similarity in heat flux, noise intensity, and turbulent velocity profile exponent in going from transitional to fully developed turbulent flow. This observation provided a convenient technique for further generalizing the form of the power spectral density function to account for transitional flow.

II. Experiment Description

The objective of this wind tunnel test program was to obtain acoustic data which could be used to verify or redefine aero-acoustic prediction methods which currently exist in the aerospace community. Tunnel operating conditions and acoustic sensor locations have been chosen such that measurements were made in regions of laminar, transitional, and turbulent flows and of base flow fluctuations.¶ Variations due to the effects of Mach number, Reynolds number, angle of attack and nose bluntness were considered.

Model

The model used in the current wind-tunnel test program is the heat-transfer model which was used on the Air Force sponsored study reported in Ref. 1. The model is a 7.2° half-angle cone with a base radius of 5.40 in. The model was constructed of 0.060 in. thick series 400 stainless steel, and incorporated changeable noses with radii of 0, 0.055, and 0.110 in. It was instrumented with 29 flush mounted and two ported microphones, and 40 backface thermocouples. A drawing defining the model configuration and the instrument locations is shown in Fig. 1.

Test Facility

The experiments were conducted in the Arnold Engineering Development Center, von Kármán Facility in Tunnels A, B, and C at Mach numbers of 4, 8, and 10, respectively. A description of these facilities may be found in Ref. 2.

¶ Although the base pressure fluctuation measurements are not included in this paper, they are included in the final report which documents the complete results of the investigation (AFFDL TR72-138, Vols. I and II).

Model Instrumentation

The model was instrumented with 40 chromel-alumel backface thermocouples which were used to define the transitional boundary-layer zone and with 31 Gulton Industries $\frac{1}{4}$ in. diam, vibration compensated, high intensity piezoelectric microphones (25 on the cone surface and 6 on the base).

All but two of the microphones were installed in an essentially flush-mounted configuration as illustrated in Fig. 1, while two microphones were installed in a ported arrangement (Fig. 1) using two different orifice lengths to obtain comparative data useful in planning flight vehicle installation. The active diameter of the microphone is 0.2 in., Corcos' criterion[3] indicates minimal corrections for gages of this diameter in the frequency range below 20 kHz.

The flush installation was chosen in order to obtain a maximum frequency response consistent with the 100 kHz self-resonant frequency of the microphone and to avoid the uncertain effects of an orifice and cavity on frequency response over a range of ambient pressures. The sensors were installed (in nylon inserts for electrical isolation) to within two or three mils of the model surface and the remaining space filled with RTV 560 silicone rubber which was smoothed to the model contour. The silicone rubber serves three purposes: first, a smooth completely flush surface is maintained; second, a degree of protection is achieved for the sensor diaphragm; and third, some filtering of pyroelectric effects on the sensor response is obtained. The pyroelectric output due to heat transfer to the crystal elements of these microphones is relatively high; however, the additional heat capacity of the RTV rubber filters out high frequency fluctuations in heat transfer to the sensor and the inclusion of low frequency cutoff at about 15 Hz in the signal conditioning minimizes any residual effects as confirmed by the test results. Temperature effects on microphone sensitivity were avoided by limiting the duration of model exposure to high-temperature flows in Tunnels B and C to periods of 10–30 sec through use of the available model insertion and retraction mechanisms.

Because of the inability of the vendor to supply microphone calibration data above 15 kHz, concern over the validity of the atmospheric calibration data in a near vacuum environment, and a desire to evaluate the effects of the RTV coating on sensor sensitivity and frequency response, shock tube tests were made. In these tests each microphone was subjected to pressure steps of about 0.1 psi and 1.0 psi from initial pressures of 0.05 psia and 0.6 psia, respectively, in order to bracket the range of actual wind tunnel test conditions. These tests confirmed that the rubber coating had little effect on sensor sensitivity within the frequency range of interest. Rise time (10–90%) of the uncapped, RTV-coated microphone was nominally 10 μsec compared to about 30 μsec when the vendor-supplied perforated cap was used.

In order to maximize the signal-to-noise ratio of the acoustic data, a single-stage field effect transitor amplifier was included in the model for each microphone. These amplifiers provided a system noise level equivalent to about 85 db of sound pressure levels (SPL) and linear to at least 180 db SPL over the frequency range from about 15 Hz to 20 kHz. All acoustic data were recorded by two AMPEX Type FR-1300 and one CEC Type 3360 magnetic tape recorders using 9-20 kHz FM recording.

Instrument Locations and Test Conditions

In order to determine the spacing of the sensors on the cone, it was necessary to establish the location of the transitional boundary-layer zone for each of the proposed test conditions. This required the correlation of available transition data for each of the three AEDC test facilities where tests were planned.

The largest single source of applicable transition data for the Mach 8 condition (Tunnel B) may be found in Ref. 1. These data were obtained for the same cone and range of test conditions that was used in the current test series. The location of onset and end of transition were deduced from the heat-transfer measurements. That is, the onset of transition was defined as the point where the heat transfer is a minimum, and the end of transition as the point where the heat transfer is locally a

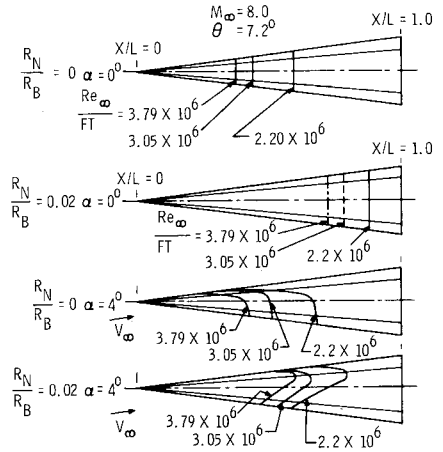

Fig. 2 Spatial distribution of end of transition with Reynolds number and angle of attack.

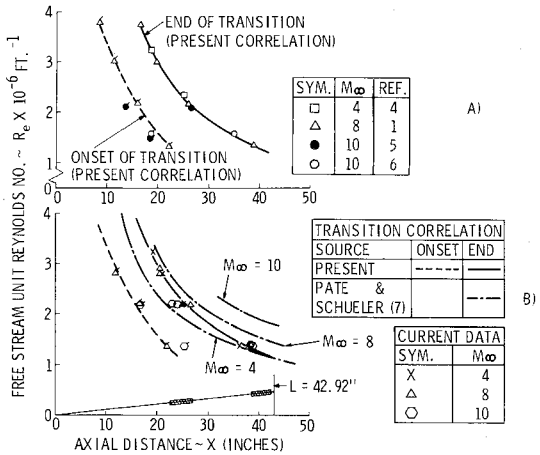

Fig. 3 Correlation for the location of the boundary-layer transition zone for the sharp cone ($\alpha = 0°$).

maximum. From these data the spatial distribution of the end of transition was deduced (from $\dot{q}_{max}$) and some typical results are repeated here in Fig. 2.

Available transition data for sharp cones for Tunnel A at Mach 4 and Tunnel C at Mach 10 may be found in Refs. 4–6. These data were used to establish the Mach number sensitivity of transition location with Reynolds number. The available data were for cone angles which were different than the 7.2° half-angle cone to be tested. The following procedure was used to establish the transition location on the test model for various freestream unit Reynolds numbers.

The local wetted length Reynolds number at transition, $(Re_s)_t \equiv [(\rho u/\mu)_e s]_t$, for the zero angle-of-attack case was computed for each data case. Where the value $(\rho u/\mu)_e$ is the local unit Reynolds number at the boundary-layer edge, evaluated at at the transition point (S_T). Then assuming that the same value of $[Re_s]_T$ would prevail for the 7.2° half-angle cone, the corresponding freestream unit Reynolds number was determined. Transition location data thus obtained are presented in Fig. 3A. It is of interest to note that the available end-of-transition data for sharp cones, collapses to a single line in this particular format, independent of the freestream Mach number. This does not imply that there is no Mach number effect on transition, but that in this particular format the effect is implicit. Note that T_w/T_{aw} varied as shown in Table 1. Furthermore, this correlation is only valid for defining transition in Tunnels A, B, and C at AEDC and should not be construed to be generally valid for all test facilities.

Table 1 Variation of T_w/T_{aw}

Facility	M_∞	Freestream Re/ft $\times 10^{-6}$	T_w/T_{aw}	R_N, in.	α, deg
A	4	1.4	1.0	0.0	0, ±1, ±2, −4, −7.2, −8.2
		2.2		0.0	0, ±1, ±2, −4, −7.2
		2.8		0.0	0, ±1, ±2, −4 −7.2
		2.2		0.055	0, ±1, ±2, −4, −7.2
	4	3.0		0.11	0, ±1, ±2, −4, −7.2
B	8	1.4[a]	0.48	0.0	0, ±1, ±2, ±4, ±7.2
		1.4		0.0	0, ±1, ±2, +7.2
		2.2		0.0	0, ±1, ±2, ±4, ±7.2
		2.8		0.0	0, ±1, ±2, ±7.2
		2.2		0.055	0, ±1, ±2, ±4, ±7.2
	8	3.25		0.11	0, ±1, ±2, ±7.2
C	10	1.4	0.30	0.0	0, −0.5, ±1, ±2, −4, −7.2
		2.2		0.0	0, −0.5, ±1, ±2, −4, −7.2
		2.2		0.055	0, ±1, ±2, −4, −7.2
		2.2		0.11	0
	10	2.2		0.0	−0.5 (with trip)

[a] Tunnel doors open, remaining tests in Tunnel B performed with Tunnel doors closed.

The correlation of Pate and Schueler[7] was also used to define the location of transition for the planned test conditions. In this reference, they developed a quantitative correlation which demonstrated a strong Mach number dependence and also indicated a variation with tunnel size and unit Reynolds number. For the three facilities considered here, the axial location of transition for each freestream Mach number, as deduced from Ref. 7, is shown in Fig. 3B. One will note that this correlation does exhibit a Mach number dependence which is not reflected in the correlation presented in this paper. At a freestream unit Reynolds number of 2.2×10^6, Pate's correlation indicates an axial location of the end of transition to be at $x \approx 21$ in. for $M_\infty = 4$ and at $x \approx 34$ in. at $M_\infty = 10$. The current criteria indicates a location of $x \approx 25$ in. independent of the Mach number. The current tests were used to resolve this apparent discrepancy. Nevertheless, the sensor locations (single and arrays) were selected to be consistent with the correlation and test conditions shown in Fig. 3A and Table 1.

The only applicable transition data available to date for the blunt body case was from Ref. 1, (i.e., for $M_\infty = 8$). The onset and end of transition data for $R_N = 0.055$ in. and $R_N = 0.110$ in. are presented in Fig. 4. Based upon the sensor locations established for the sharp cone, the test conditions for the blunted cone were selected to provide a fixed location of transition as noted in Fig. 4.

Because of the paucity of blunt cone transition data on cones at Mach 4 and 10, it was assumed that the Mach 8 data of Ref. 1 are representative of the bluntness effect. The validity of this assumption was to be verified by the current tests.

Summary of Data Obtained

Tests were conducted at freestream Mach numbers of 4, 8, and 10, respectively, with corresponding wall-to-adiabatic wall temperature ratios of 1.0, 0.48 and 0.30, respectively. Since the

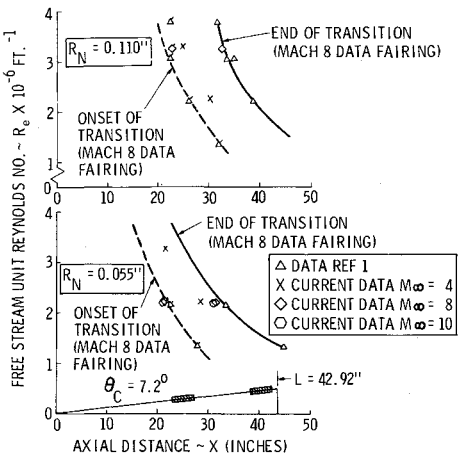

Fig. 4 Correlation for the location of the transition boundary-layer zone for the blunted cones ($\alpha = 0°$).

instrumentation is located predominantly along one conical ray, data were obtained with this ray on both the leeward and windward sides of the model (i.e., for both $\pm$ angles of attack). Table 1 presents the freestream conditions for which data were obtained. The $-\alpha$ condition implies data on the windward ray.

III. Presentation of Results

Transition Shape Data

Heat-transfer data defining the shape of the transition front were obtained at Mach 8 and 10 along three conical rays. As mentioned earlier, the location of transition onset was defined as that point where the heat transfer (i.e., Stanton number) is a minimum. The end of transition was defined as the point where the heat transfer is locally a maximum. For the zero angle of attack case, comparisons of these data with the current design correlation is shown in Figs. 3B and 4 for $R_N = 0$ and $R_N \neq 0$, respectively. Good agreement of the test data with the correlation proposed herein is noted. Furthermore, the data do not exhibit the Mach number sensitivity evident in Pate and Schueler's correlation.[7]

At Mach 4 where the low stream total temperature (120°F) precluded the measurement of heat transfer with thermocouples, thermographic phosphorescent paint was used to establish the transition zone. For these measurements a thin coating of phosphor paint was sprayed on to a fiberglas shell which was to fit over the basic steel model. The phosphorescent paint technique[8] consists of photographing the painted model surface and measuring the optical density of the recorded image. The optical density of a photographic image is a function of the

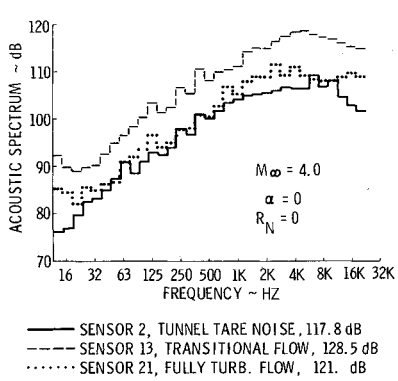

Fig. 5 Pressure spectrum vs flow condition for three typical gages (Re_∞/ft = 2.2 × 10^6).

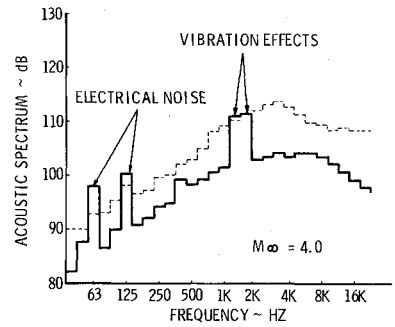

Fig. 6 Comparison of compensated and poorly compensated microphones.

logarithm of the intensity of the exposure, for a given exposure time. If the exposure from the phosphorescent paint falls within the logarithmically linear region, the optical density will be a function of the ultraviolet (u-v) light intensity and the emitted light intensity of the paint. For these wind tunnel tests, the procedure was to take a photograph of the model before the tunnel run (i.e., a tare) and then take another one during the run. It suffices to say that the incremental change in optical density is proportional to the surface heat transfer. In the present case we were not searching for the absolute level of the heat transfer but for those points where it reached a minimum (transition onset)or a maximum (transition end). Due to the limited region of photographic coverage, only the end of transition data were obtained. These results are also shown in Figs. 3B and 4. For the sharp cone excellent agreement with the current correlation is noted. For the blunted cone, the Mach 4 data indicate that the end of transition, for a given freestream Reynolds number, is further forward than for the comparable Mach 8, 10 case. Comparisons of the end of transition from heat transfer and phosphor paint were made at Mach 8 and the data indicate that the two are in excellent agreement.

Acoustic Pressure Data

Fluctuating pressure data were obtained for several angles of attack, at each test Mach number and Reynolds number, as defined in Table 1. For screening purposes, the acoustic data were reduced using third octave band analysis. Figure 5 represents typical data obtained in tunnel A at Mach 4. Sensor 2 located in the nose section is representative of tunnel tare noise at this test condition, since laminar flow occurs over this gage. Sensor 13 located in the forward array represents the pressure distribution during transitional flow, while sensor 21 located in the aft array represents turbulent flow. Tunnel tare noise will not have a dominant effect on data taken during transitional flow because of the high signal to noise ratio present. The data that were obtained are being analyzed for the SPL as well as cross-spectral and cross-correlation functions. To assess tunnel noise effects, cross correlation and coherence functions must be determined between sensors in laminar and turbulent flow. Data in the laminar region should have a high degree of correlation. Between laminar and turbulent flow, data should be uncorrelated. These analyses will not be included in the current paper, rather, SPL data will be presented.

Although the piezoelectric microphones are vibration compensated, effects were noted which indicate that certain gages were not sufficiently compensated to eliminate vibration effects. Shown in Fig. 6 are comparisons of a poorly compensated gage vs a well compensated gage. Adjustments were made to vibration-affected data to eliminate the resonant peaks caused by these effects. These corrections were required for data from approximately 10 gages.

Shown in Figs. 7 and 8 are the longitudinal variations of the SPL (0–20 kHz), with freestream Reynolds number (i.e., transition region) at Mach 4 and 8, respectively. At Mach 4, peak

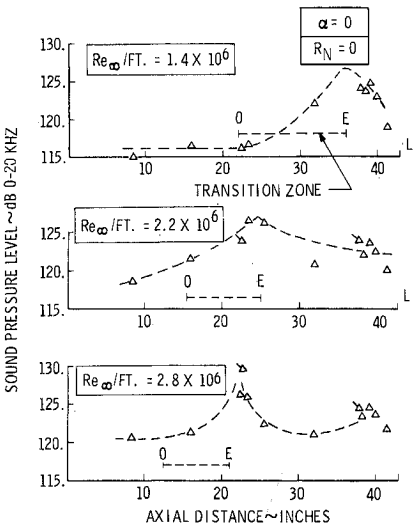

Fig. 7 Effect of freestream Reynolds number on sound pressure level ($M_\infty = 4$).

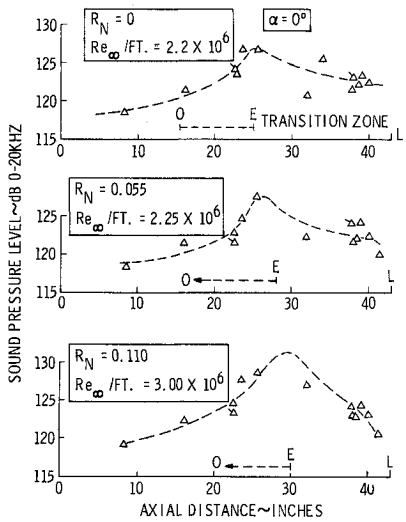

Fig. 9 Effect of bluntness on sound pressure level (M_∞ 4).

RMS pressure levels are approximately 10 db higher than indicated by the sensor located in the laminar boundary layer, while at Mach 8 the corresponding increment is approximately 5 db. Fully turbulent pressure levels are approximately 3 to 4 db above laminar boundary-layer noise levels at both Mach 4 and 8. Two items of interest should be noted about the laminar boundary-layer noise levels: 1) there is roughly a 5 db increase at Mach 8 over the level at Mach 4 for the same freestream Reynolds number; thus the laminar boundary-layer noise level apparently increases with increased Mach number (i.e., pressure level), and 2) in the current tests, the laminar measurements were made at the same test conditions for which the turbulent data were obtained. With regard to this latter comment, it is somewhat confusing in reported data to find that the laminar boundary-layer noise levels were established by lowering the freestream Reynolds number so that the sensor is immersed in laminar flow. Clearly this would not be the same noise level for the reported turbulent data and should not be confused with the value that would be measured at the turbulent or higher Reynolds number test conditions.

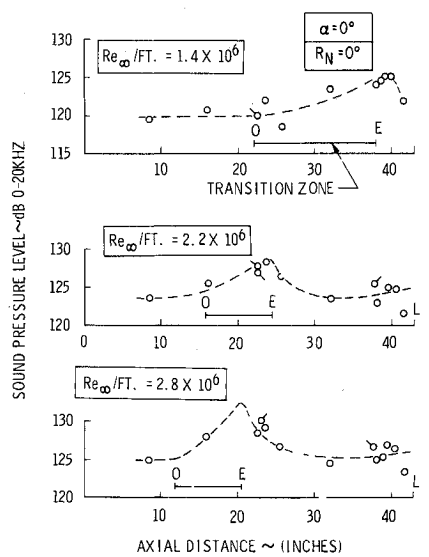

Fig. 8 Effect of freestream Reynolds number on sound pressure level ($M_\infty = 8$).

Shown in Fig. 9 is the effect of bluntness on the overall sound pressure level at Mach 4. For this comparison, the freestream conditions were selected so that the location of the end of transition is nominally fixed on the model surface. It is evident from this figure that, for the range investigated, there is no definite effect of bluntness, per se, on the sound pressure level and distribution, although it was shown that bluntness does have an effect on transition location. The effect of angle of attack (windward ray) on the sound pressure level distribution at Mach 4 is shown in Fig. 10. The axial trend that is evident for the zero alpha case persists for the nonzero alpha cases, however, the distribution apparently shifts axially with the transition zone. A sampling of the windward vs the leeward distribution of the SPL at $\alpha = \theta_c = 7.2°$ is presented in Fig. 11. It is interesting to

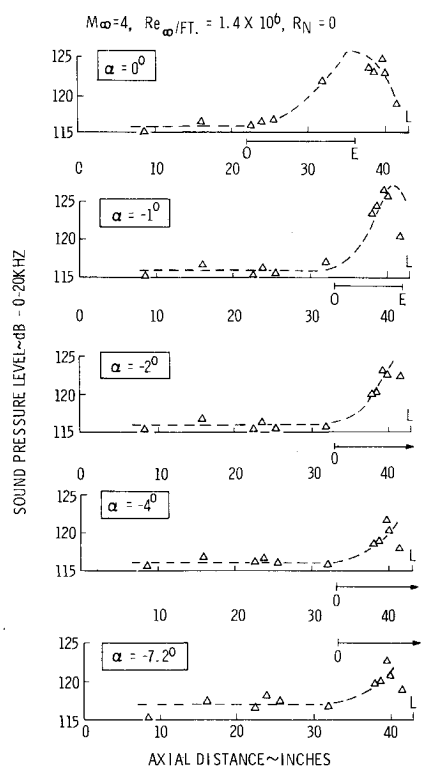

Fig. 10 Effect of angle of attack on sound pressure level.

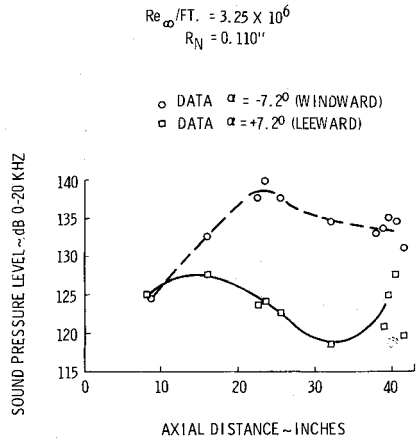

Fig. 11 Windward vs leeward distributions of the sound pressure level for $M_\infty = 8$.

note the relatively large levels of the SPL on the windward ray while for the leeward ray, the levels drop below the laminar boundary-layer noise levels then increase near the base. This increase could be attributed to upstream influences of the base flow in the separated flow region. The large variation between the wind and leeward rms pressure levels should be of interest to the designers of maneuvering vehicles since the large peripheral distribution must be factored into the vehicle design. The leeside data with the exception of the data of Fig. 11, will not be presented in this paper.

The increase in the rms sound pressure level near the end of transition evident in the current data and also in the data of Pate[9] is similar to that increase in the velocity profile exponent, n, measured by Martellucci,[10] on a sharp 7.25° half-angle cone. Comparisons of the axial distribution of the measured heat transfer and the over-all sound pressure level data obtained in the current study with the velocity profile exponent results of Ref. 10 are shown in Fig. 12. Turbulent boundary-layer velocity profiles

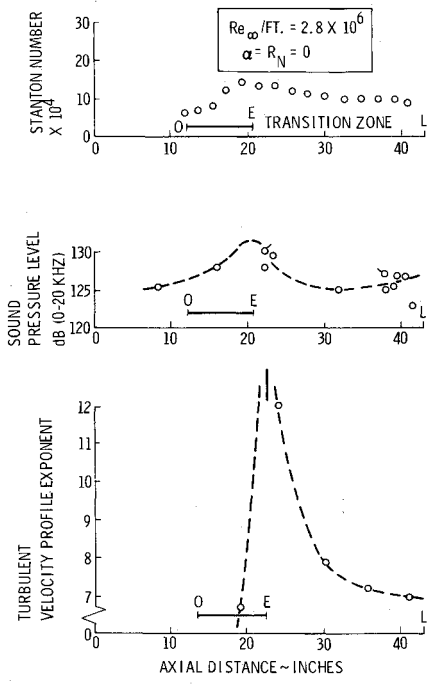

Fig. 12 Comparison of the axial distribution of the heat transfer, rms sound pressure level and the turbulent velocity profile exponent ($M_\infty = 8$).

are customarily characterized by the power-law relation $u/u_e = (y/\delta)^{1/n}$. The exponent, n, was obtained by measuring the slope of the velocity profile plotted on log-log paper in the range $0.1 \leqq y/\delta \leqq 0.9$. It should be noted that the increase in n was noted by other experimenters.[11] It is evident from Fig. 12 that there is a commonality in the axial distributions of all three parameters. The implication of this increase on the rms prediction method of Lowson[12] and Houbolt[13] will be discussed in the next section.

IV. Discussion of Results

Considerable data have been generated in the measurement of turbulent boundary-layer properties for subsonic flows. These data have been utilized to predict sound pressure levels and associated spectra for the subsonic case. For supersonic and hypersonic flows, a paucity of data exist for naturally formed turbulent flows (i.e., sans boundary-layer trips). There have been some limited flight test data obtained, but these must be viewed with caution because of the many uncertainties associated with the exact environment and the measuring techniques. Lowson[12] and Houbolt[13] have both postulated methods for determining the supersonic sound pressure levels and spectra for fully developed attached turbulent boundary layers. These theories are predominantly based upon the available low-speed ground test data. Lowson[12] proposes that the ratio of the over-all rms pressure fluctuation ($\tilde{p}$) to the local edge dynamic pressure (q_e) for fully developed turbulent flow can be determined from the following relation:

$$\tilde{p}/q_e = 0.006/[1+0.14M_e^2] \tag{1}$$

which compares with that postulated by Houbolt[13]

$$\tilde{p}/q_e = 0.007/[1+0.012M_e^2] \tag{2}$$

For a sharp cone, where the edge Mach number and dynamic pressure are constant, Eqs. (1) and (2) predict that the rms pressure is constant in the turbulent region. However, one will note from Figs. 7–12 that the rms pressure achieves a maximum at the end of transition (i.e., the point defined by a maximum in the local $\dot{q}$). The region downstream of this point is customarily called the turbulent boundary-layer region. As pointed out by Martellucci[10] and shown in Fig. 12, a region exists downstream of the customarily defined end of transition where strong nonsimilar effects are present. At Mach 8, this region persists for some 50 to 100 boundary-layer thicknesses downstream. Owen and Horstman[14] in their recent publication also address this phenomena in a somewhat different manner. They postulate that the transitional region does not end at the point where the turbulent fluctuations, heat transfer, rms sound pressure level, profile exponent, etc. peak, but that it also encompasses what is referred to here as the nonsimilar region. This is a somewhat different viewpoint and represents an area where insufficient data and analytic modeling exist to characterize this flow phenomena in any detail. Nevertheless, in order to predict the rms pressure in this nonsimilar region, it is suggested that Eq. (1), for example, be modified so that

$$\tilde{p}/q_e = F(n)/[1+0.14M_e^2] \tag{3}$$

When $n \approx 7.0$, $F = 0.006$ and when $n > 7$ then $F > 0.006$. What must then be established is a means of determining the axial variation of n. The intent here is to provide a possible means of modifying the turbulent relations to provide a design-technique for predicting rms pressures in this transitional region. It is obvious that this is an area that requires additional research.

The rms pressure levels for fully developed turbulent flow predicted by Lowson[12] [Eq. (1)] and Houbolt[13] [Eq. (2)] are compared to one set of data** (Re_∞/ft $= 2.2 \times 10^6$, $R_N = 0$) over the Mach number range investigated and are shown in Fig. 13. Lowson's method[12] tends to underpredict at the higher Mach numbers and somewhat overpredicts for the $M_\infty = 4$ case

** The energy associated with frequencies 20 kHz $\leqq \phi \leqq \infty$ were added to the data using the analytic form of Houbolt.[13]

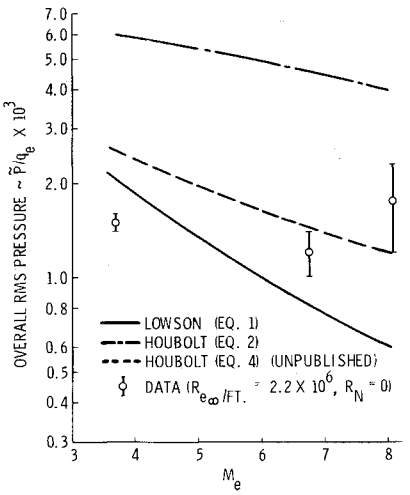

Fig. 13 Comparison of theory with fully developed turbulent boundary-layer data.

($M_e = 3.69$). Houbolt's method[13] clearly overpredicts the rms pressure levels over the entire Mach number range investigated. In order to resolve this discrepancy, which relates predominantly to the Mach number coefficient in the denominator, Houbolt has recently further generalized his work (unpublished). The following form is postulated:

$$\tilde{p}/q_e = 0.007/[1+r_e(\gamma-1/2)M_e^2] \tag{4}$$

where

$$r_e = [1-(u_L/u_e)][r_i+(u_L/u_e)]$$

and

$$r_i = 2[(T_w/T_e)-1]/[M_e^2(\gamma-1)]$$

The parameter u_L is the local velocity at the edge of the laminar sublayer. This can be expressed as

$$u_L/u_e = 10.5[(T_w/T_e)(c_f/2)]^{1/2}$$

The results from Eq. 4 are also shown in Fig. 13. This method predicts well at the higher Mach numbers but overpredicts somewhat at Mach 4.

Tunnel/Laminar Boundary-Layer Moise

Some observations pertaining to the laminar tunnel boundary-layer noise levels are in order. Donaldson and Wallace[15] noted in their report that the acoustic measurements on the surface of the flat plate revealed pressure fluctuation levels larger than those of the freestream by a factor of at least 20. These data were obtained at $M_e = 4$. Measurements by Kendall[16] show that disturbances at all frequencies grow monotonically from the leading edge, and the source of these disturbances has been identified as the sound field radiated from the tunnel wall boundary layer. In a more recent publication, Kendall[17] presents additional flat plate and cone experimental data. In this reference it is indicated that for $M_\infty = 4.5$ and possibly for $M_\infty = 3.0$ the tunnel sound field forces fluctuating energy into the boundary layer in a region immediately aft of the leading edge of the test plate. The energy is observed to grow severalfold larger ahead of the station for which stability theory predicts the onset of amplification. Thus the sound field must actively interact with the boundary layer to provide the observed growing disturbances. In a recent publication, Mack[18] presents numerical results which give not only details of the response of the boundary layer to an external sound wave, but also the strength of the reflected sound wave and pressure fluctuation level at the wall. It was shown that the sound field which radiates from the turbulent boundary layer on the nozzle walls and which reflects off of the model can indeed be amplified. Furthermore Fischer and Weinstein[19] noted that a region exists upstream of the classical point on the body surface where the heat transfer begins to rise (i.e., classically called transition onset) where the outer portions of the boundary layer are turbulent and the inner region has a laminar like behavior. The initial disturbance begins at the critical layer and then spreads to the wall. These authors determined that the spreading angle relative to the wall was relatively constant, that is $\phi_{\text{wall}} = 0.5° \rightarrow 1.0°$ for $M_e = 2.5 \rightarrow 13.6$. Since the location of the critical layer moves outward in the boundary layer with increasing Mach number,[20] the relatively constant spreading angle implies a greater upstream influence of boundary-layer transition as Mach number increases. Thus a microphone located at a point upstream of the location of transition on the surface but in the Mach cone of influence of the turbulent boundary layer would indicate a higher sound level than the freestream. As Owen and Horstman[14] have pointed out, this could be related to the uncertain definition of what is classically called the transitional boundary-layer region.

The laminar sensors on the forward portion of the model in the current study were located in this region of influence. Thus the laminar boundary-layer noise levels referred to earlier are actually combined measurements of tunnel noise plus the additional noise associated with the amplification associated with laminar boundary-layer flows. This helps to explain the unusually high background or noise levels observed in the current tests.

V. Summary of Results

Fluctuating pressure and heat-transfer measurements were obtained on a slender cone at Mach numbers of 4, 8, and 10. Data were obtained for a range of freestream Reynolds numbers (transition locations), cone bluntness ratios, and for an angle of attack range of 0 to 7.2° (the cone half-angle). The fluctuating pressure measurements were obtained with vibration compensated, high intensity piezoelectric microphones over frequency range of 0 to 20 kHz. Natural transition (i.e., sans trips) occurred in all cases. The results presented indicate that maximum surface pressure fluctuation intensities occur near the end of transition, defined as the point where the local surface heat transfer is a maximum. Furthermore, it was shown that there is a similarity in the axial distribution of the heat transfer, rms pressure, and the velocity profile exponent. It is proposed that this similarity can be utilized to modify the predictions of the rms distribution from transitional flows to regions of fully developed turbulent flows.

References

[1] Martellucci, A., "Asymmetric Transition Effects on the Static Stability and Motion History of a Slender Vehicle," SAMSO-TR-70-141, Jan. 1970, U.S. Air Force, El Segundo, Calif.; also *Journal of Spacecraft and Rockets*, Vol. 8, No. 5, May 1971, pp. 476–482.

[2] *Test Facilities Handbook, AEDC*, 7th ed. Arnold Air Force Station, Tenn., 1968.

[3] Corcos, G. M., "Resolution of Pressure in Turbulence," *Journal of the Acoustical Society of America*, Vol. 35, No. 2, Feb. 1963, pp. 192–199.

[4] Pate, S. R., "Measurements and Correlations of Transition Reynolds Numbers on Sharp Cones at High Speeds," AEDC TR-69-172, Dec. 1969, Arnold Engineering Development Center, Arnold Air Force Station, Tenn.

[5] McCauley, W. D., Saydah, A., and Bueche, J., "Effect of Spherical Roughness on Hypersonic Boundary-Layer Transition," *AIAA Journal*, Vol. 4, No. 12, Dec. 1966, pp. 2142–2148.

[6] DiCristina, V., "Three-Dimensional Laminar Boundary-Layer Transition on a Sharp 8° Cone at Mach 10," *AIAA Journal*, Vol. 8, No. 5, May 1970, pp. 852–856.

[7] Pate, S. R. and Schueler, C. J., "Radiated Aerodynamic Noise Effects on Boundary-Layer Transition in Supersonic and Hypersonic Wind Tunnels," *AIAA Journal*, Vol. 7, No. 3, March 1969, pp. 450–457.

[8] Knox, E., private communication, Jan. 1972, ARO Inc., Tullahoma, Tenn.

[9] Pate, S. R. and Brown, M. D., "Acoustic Measurements in Supersonic Transitional Boundary Layers," Paper 1.3.1, presented at the

15th ISA Aerospace Instrumentation Symposium, May 1968; also AEDC TR-69-182, 1969, Arnold Engineering Development Center, Arnold Air Force Station, Tullahoma, Tenn.

[10] Martellucci, A., "Effects of Mass Transfer on Hypersonic Turbulent Boundary-Layer Properties," *AIAA Journal*, Vol. 10, No. 2, Feb. 1972, pp. 181–187.

[11] Johnson, C. B. and Bushnell, D. M., "Power-Law Velocity Profile and Mach Number in a Turbulent Boundary Layer," TND-5753, April 1970, NASA.

[12] Lowson, M. V., "Predictions of Boundary Layer Pressure Fluctuations," AFFDL-TR-67-167, April, 1968, Air Force Flight Dynamics Lab., Wright-Patterson Air Force Base, Ohio.

[13] Houbolt, J. C., "On the Estimation of Pressure Fluctuations in Boundary Layers and Wakes," GE-TIS 66SD296, Aug. 1966, General Electric Co., Philadelphia, Pa.

[14] Owen, F. K. and Horstman, C. C., "Hypersonic Transitional Boundary Layers," *AIAA Journal*, Vol. 10, No. 6, June 1972, pp. 769–775.

[15] Donaldson, J. C. and Wallace, J. P., "Flow Fluctuations Measurements at Mach Number 4 in the Test Section of the 12-Inch Supersonic Tunnel," AEDC-TR-71-143, Aug. 1971, Arnold Engineering Development Center, Arnold Air Force Base, Tullahoma, Tenn.

[16] Kendall, J. M., Jr., "Supersonic Boundary Layer Transition Studies," *Space Programs Summary 37–62*, Vol. III, J. P. L. Propulsion Lab., Pasadena, Calif., 1970.

[17] Kendall, J. M., Jr., "J. P. L. Experimental Investigations," *Proceedings of the Boundary Layer Transition Workshop*, SAMSO-Dec. 1971, pp. 2-1 to 2-16.

[18] Mack, L. M., "Progress in Compressible Boundary Layer Stability Computations," *Proceedings of the Boundary Layer Transition Workshop*, Aerospace Corp., Dec. 1971, pp. 1-1 to 1-35.

[19] Fischer, M. C. and Weinstein, L. M., "Come Transitional Boundary-Layer Structure at $M_e = 14$," *AIAA Journal*, Vol. 10, No. 5, May 1972, pp. 699–701.

[20] Stainback, P. C., "Use of Rouse's Stability Parameter in Determining the Critical Layer Height of a Laminar Boundary Layer," *AIAA Journal*, Vol. 8, No. 1, Jan. 1970, pp. 173–175.

MAY 1973 AIAA JOURNAL VOL. 11, NO. 5

Aerodynamics of High-Performance Ludwieg Tubes

DAVID A. RUSSELL* AND KWOK-ON TONG†
University of Washington, Seattle, Wash.

A small perturbation analysis of the flow in a Ludwieg tube supply is described which includes both the growing turbulent boundary layer and pipe axial nonuniformities. Measured pressure time histories are used to check the theory and its extension to high pipe Mach numbers and large flow perturbations. The nonsteady coupling of this flow to a nozzle is investigated. Calculations are made of the effects on the nozzle boundary layer, while a separate analysis is carried out for the case of complete mixing in a nozzle plenum. The double expansion nozzle is shown to extend Ludwieg tube capability. Analytical and experimental studies are made of aerodynamic problems that can arise in these nozzles.

Nomenclature

A = geometric cross-sectional area (refers to test section unless otherwise indicated)
a = speed of sound
D = orifice plate hole spacing
d = pipe diameter
L = supply tube length
M = flow Mach number (refers to test section unless otherwise indicated)
p = static pressure
Re = Reynolds number of test flow (based on suitable length)
s = wave fixed coordinate (Figs. 2 and 3)
T = static temperature
t = time
U = single speed assigned to expansion wave (equal to a_4 for small M_3)
u = flow velocity in axial direction
V = staged nozzle volume between A_{op}* and A*
x = coordinate in axial direction
γ = ratio of specific heats
Δ = perturbation
δ* = boundary-layer displacement thickness (given by Fig. 2)
δ_s* = boundary-layer displacement thickness in wave fixed coordinates (equal to $M_3\delta$* for Becker model at small M_3)
ε = boundary-layer total energy thickness
θ = boundary-layer momentum thickness
ρ = static density

Subscripts
e = core flow value (radial variations neglected)
eff = effective value (including boundary-layer effects)
o = stagnation value (refers to test section unless otherwise indicated)
op = orifice plate value
p = plenum exit value
rms = root-mean-square of fluctuation
3 = unperturbed flow behind expansion wave
4 = initial conditions in the supply

Superscript
* = throat value (refers to test section unless otherwise indicated)

Presented as Paper 72-994 at the AIAA 7th Aerodynamic Testing Conference, Palo Alto, Calif., September 13–15, 1972; submitted September 25, 1972; revision received December 26, 1972. This work was supported by NASA Grant NGR 48-002-107. The authors would like to acknowledge valuable contributions from V. Buonadonna, C. Padova, L. J. Runyan, and J. Wai. The starting time of double nozzles was worked out in collaboration with T. G. Jones of Mathematical Sciences Northwest Inc.

Index categories: Aircraft and Component Wind Tunnel Testing; Nozzle and Channel Flow; Boundary Layers and Convective Heat Transfer—Turbulent.

* Associate Professor, Department of Aeronautics & Astronautics. Associate Fellow AIAA.

† Graduate Student, Department of Aeronautics & Astronautics.

Introduction

LUDWIEG tubes offer a convenient way of producing high-mass-flux aerodynamic test flows. As shown on the upper sketch of Fig. 1, a Ludwieg tube consists essentially of a long